Molecular Cell, Volume *68*

Supplemental Information

Structural Basis for Polyproline-Mediated Ribosome Stalling and Rescue by the Translation Elongation Factor EF-P

Paul Huter, Stefan Arenz, Lars V. Bock, Michael Graf, Jan Ole Frister, Andre Heuer, Lauri Peil, Agata L. Starosta, Ingo Wohlgemuth, Frank Peske, Jiří Nováček, Otto Berninghausen, Helmut Grubmüller, Tanel Tenson, Roland Beckmann, Marina V. Rodnina, Andrea C. Vaiana, and Daniel N. Wilson

SUPPLEMENTAL FIGURES

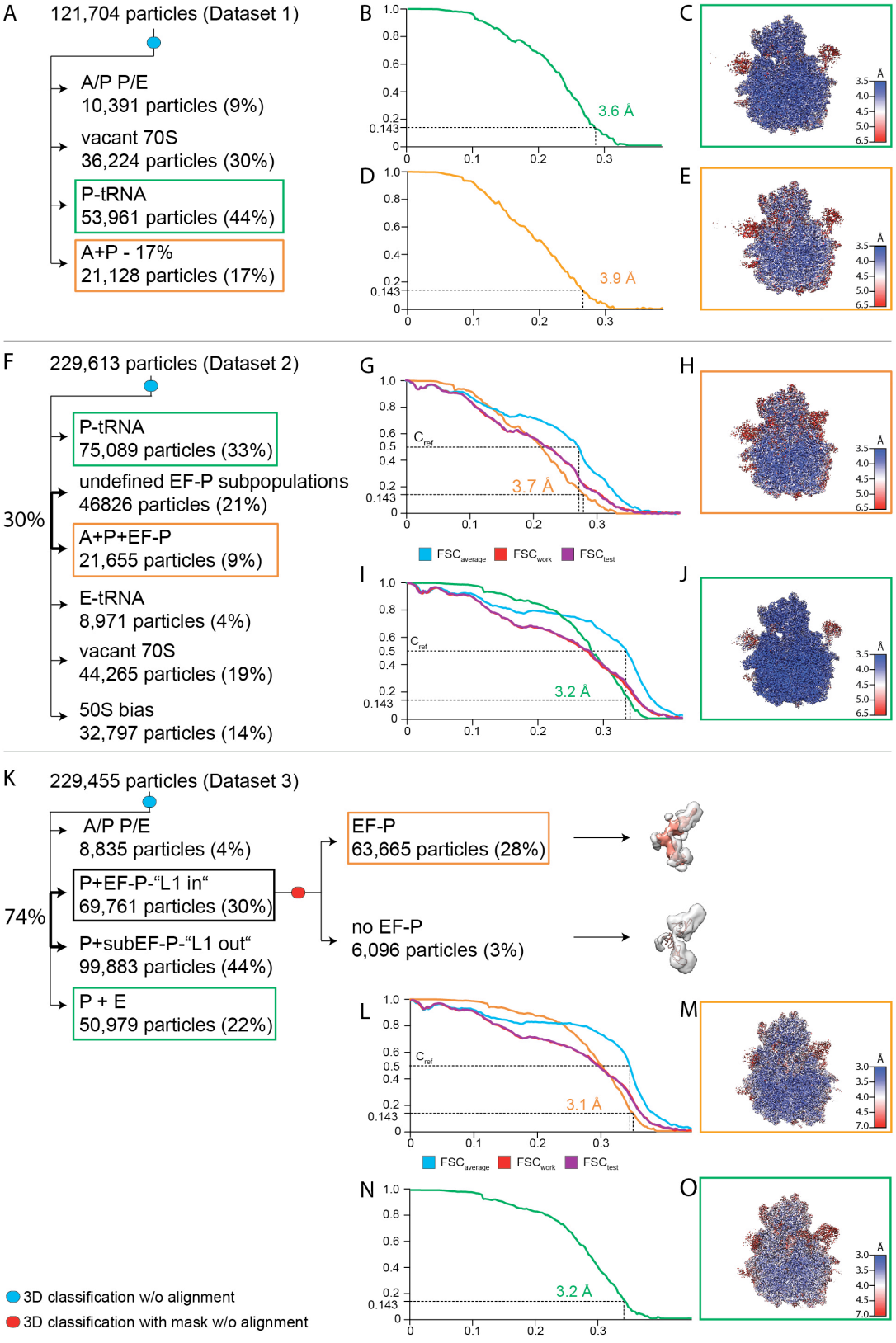

Figure S1 - Related to Figure 1-3. Data processing of the cryo-EM structures of polyproline-stalled ribosomes ± EF-P. (A) *In silico* sorting procedure for Dataset 1 derived from the PPP-stalled ribosome complexes prepared in the absence of EF-P. (B) Fourier-shell-correlation (FSC) curve (green) and (C) transverse section of the P-site tRNA only structure colored according to local resolution. (D) FSC curve (orange) and (E) transverse section of the A- and P-site tRNAs containing structure colored according to local resolution. In (B) and (D), the resolution at FSC=0.143 is indicated with a dashed line. (F) *In silico* sorting procedure for Dataset 2 derived from the PPP-SRC prepared in the presence of EF-P. (G) FSC curve (orange), as well as self and cross-validated correlations FSC_{work} (red) and FSC_{test} (purple), respectively. The resolutions at FSC=0.143 and FSC=0.5 (C_{ref}) are indicated with dashed lines. (H) Transverse section of the A- and P-site tRNA- and EF-P-containing structure colored according to local resolution. (I) FSC curve (green), as well as self and cross-validated correlations as in (G) but for the P-site tRNA only structure. (J) as (H) but for P-site tRNA only structure. (K) *In silico* sorting procedure for Dataset 3 derived from the PP-SRC prepared in the presence of EF-P. (L) FSC curve (orange), as well as self and cross-validated correlations FSC_{work} (red) and FSC_{test} (purple), respectively. The resolutions at FSC=0.143 and FSC=0.5 (C_{ref}) are indicated with dashed lines. (M) Transverse section of the P-site tRNA and EF-P structure colored according to local resolution. (N) FSC curve (green) for the P- and E-site tRNA containing structure. (O) as (M) but for P- and E-site tRNA containing structure.

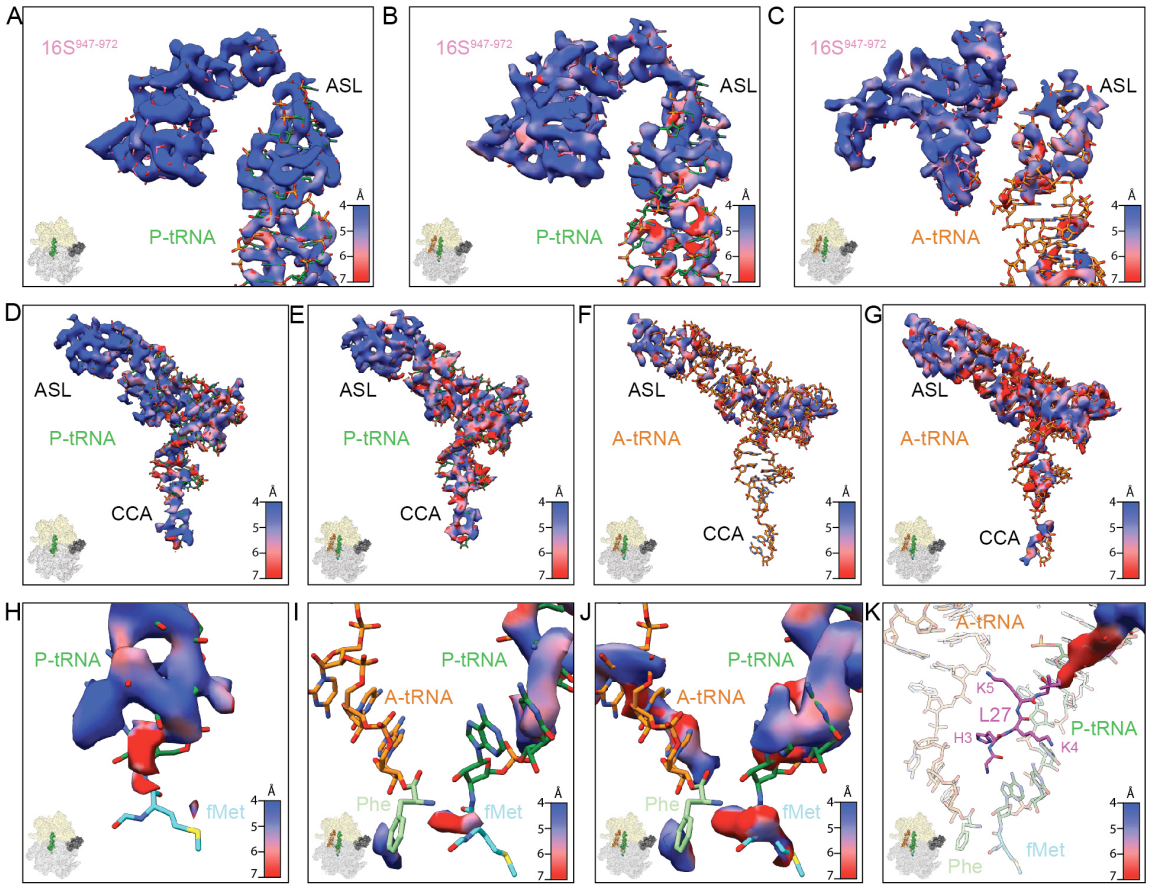

Figure S2 - Related to Figure 1. Flexibility of tRNA^{Pro} in A- and P-sites in the absence of EF-P. (A-C) Cryo-EM densities coloured according to local resolution of the ASL of P-site tRNA^{Pro} (green) or A-site tRNA^{Pro} (orange) in comparison to nucleotides 947-972 (purple) of the 16S rRNA at high threshold (7σ). (D-G) Cryo-EM densities of (D and E) P-site tRNA^{Pro} (green) and (F and G) tRNA^{Pro} (orange) coloured according to local resolution at (D-F) high (7σ) or (G) low threshold (3.5σ). (H-J) Cryo-EM densities of the CCA-ends of (H) P-site tRNA or (I and J) P- and A-site tRNAs including modeled fMet (cyan) and Phe (green) (from PDB: 1V4Y) (Polikanov et al., 2014), coloured according to local resolution. (K) Cryo-EM density colored according to local resolution for the N-terminus of ribosomal protein L27 (purple).

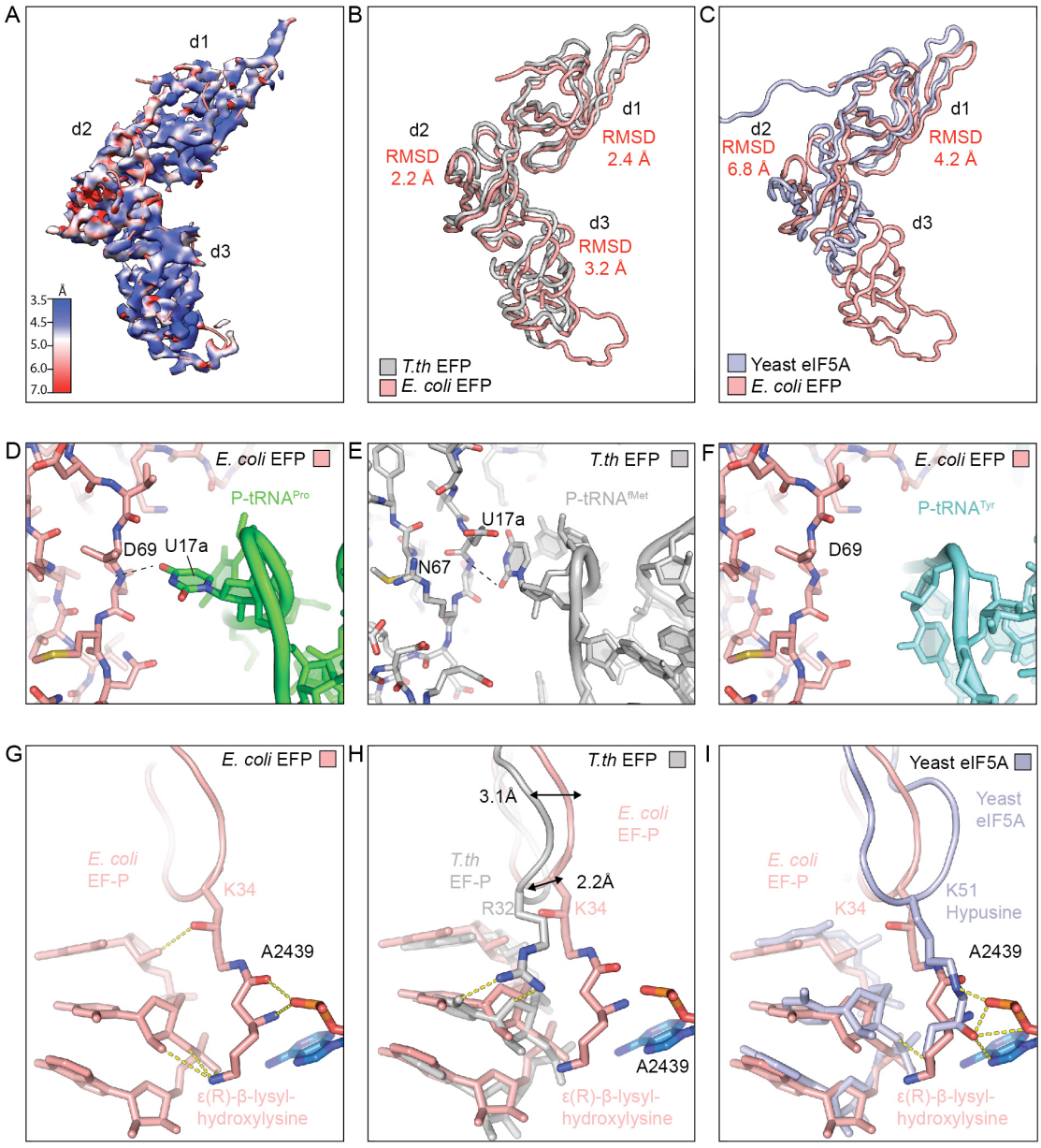

Figure S3 - Related to Figure 4. Comparison of *E. coli* EF-P, *T. thermophilus* EF-P and yeast eIF5A on the ribosome. (A) Cryo-EM density for EF-P coloured according to local resolution, with EF-P domains labeled (d1-d3). (B and C) Superimposition of ribosome-bound conformations of *E. coli* EF-P (salmon) with (B) *T. thermophilus* EF-P (grey) (PDB: 3HUX) (Blaha et al., 2009) and (C) yeast eIF5A (light blue) (PDB: 5GAK)(Schmidt et al., 2016). Root mean square deviations (RMSD) for the individual domains are indicated. (D) Interaction of D69 of *E. coli* EF-P with nucleotide U17a of the

D-loop of P-site $tRNA^{Pro}$ (green). (E) Interaction of N67 of *T. thermophilus* with nucleotide U17a of the D-loop of P-site $tRNA^{fMet}$ (grey)(PDB: 3HUX) (Blaha et al., 2009). (F) Absence of interaction of D69 of *E. coli* EF-P with the D-loop of a $tRNA^{Tyr}$ (cyan, PDB: 4WQ1) modeled into the P-site of the ribosome. (G-I) Interaction of (G) *E. coli* EF-P, (H) *T. thermophilus* EF-P (grey)(PDB: 3HUX) (Blaha et al., 2009) and (I) yeast eIF5A (light blue) (PDB: 5GAK) (Schmidt et al., 2016), with the CCA-end of P-site tRNA as well as A2439 (blue) of 23S rRNA (A2808 of 28S rRNA in yeast).

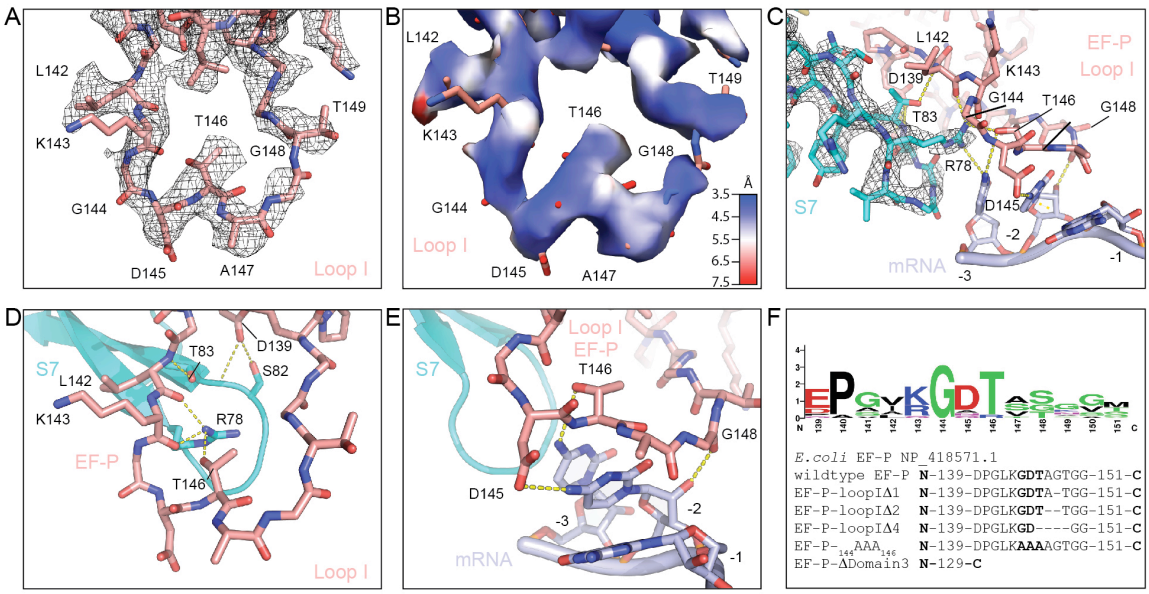

Figure S4 - Related to Figure 4. Interactions of Loop I of domain 3 with S7 and the E-site codon. (A) Electron density (grey mesh) for loop I of domain 3 (salmon). (B) Same as (A) but coloured according to local resolution. (C) Potential hydrogen bonds between loop I of EF-P (salmon), S7 (cyan) and the E-site codon (light blue) are indicated as dashed lines. (D) as (C) but only focusing on interactions between S7 and loop I of EF-P. (E) as (C) but only focusing on the interactions between the E-site codon and loop I. In (C) and (E), -1, -2 and -3 nucleotides of the E-site codon are relative to the first position of the P-site codon. (F) Weblogo of residues of EF-P loop I (based on 12 different bacterial EF-P sequences) and mutation scheme for EF-P variants.

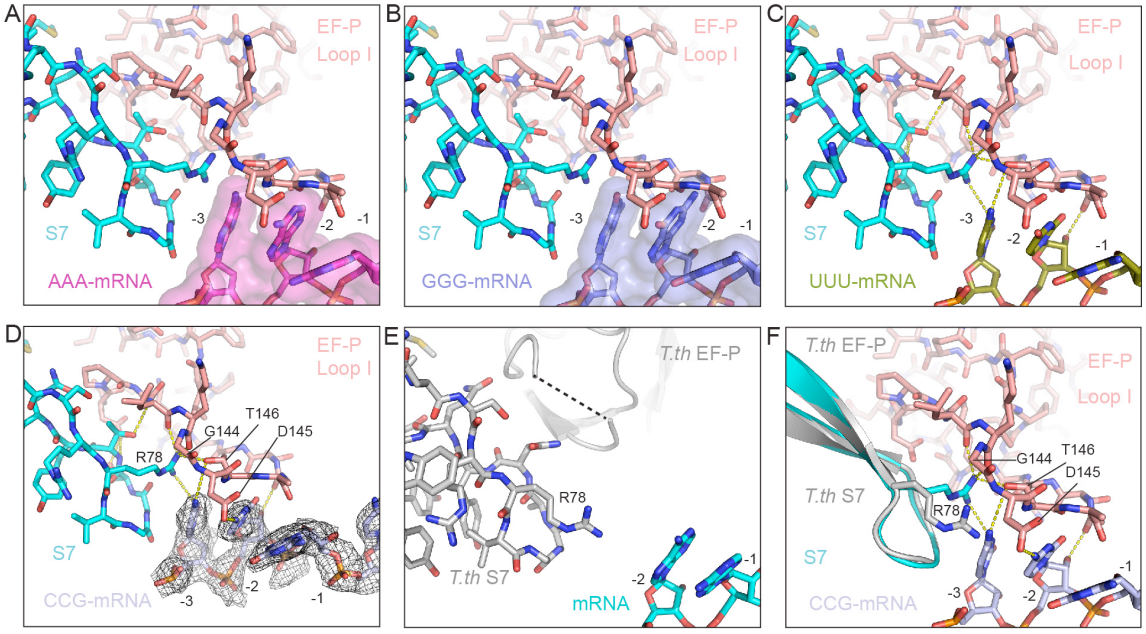

Figure S5 - Related to Figure 4. Interaction of Loop I of EF-P with the E-site codon. (A and B) Modeling of an (A) AAA (magenta) or (B) GGG (blue) codon in the E-site suggests a steric clash with residues within loop I of EF-P (salmon). (C and D) Interaction of (C) UUU (olive) or (D) CCG (light blue) codon in the E-site with loop I of EF-P and S7 (cyan). Potential hydrogen bonds are indicated with dashed yellow lines. Note an additional interaction of loop I of EF-P with the -2 position of the (D) proline codon CCG, as compared with (C) phenylalanine UUU codon. (E) Lack of interaction of *T. thermophilus* (grey) loop I of EF-P with S7 and mRNA (PDB: 3HUX) (Blaha et al., 2009). (F) Comparison of position of R78 of S7 (grey) from the *T. thermophilus* EF-P (grey) 70S structure (PDB: 3HUX) (Blaha et al., 2009) or S7 (cyan) from our *E. coli* EF-P-PP-70S structure.

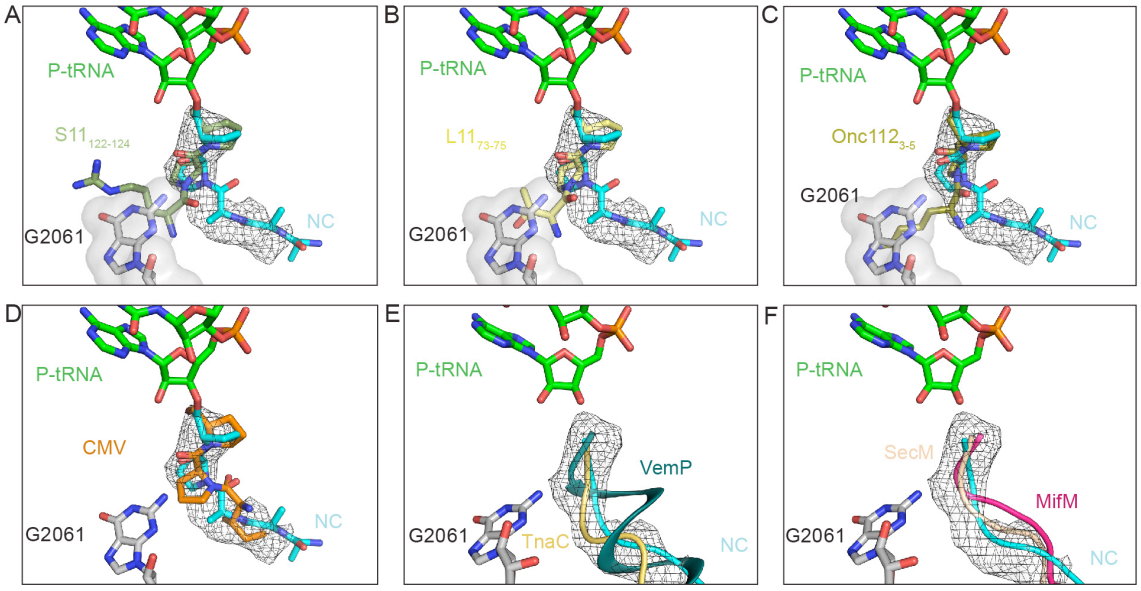

Figure S6 - Related to Figure 5. Conformation of polyproline nascent chain on the ribosome. (A-D) Comparison of cryo-EM density (mesh) and model for Pro-Pro nascent chain (cyan) compared with conformation of diprolyl residues found in (A) S11 (residues 122-124, deep olive), (B) L11 (residues 73-75, yellow), (C) the antimicrobial peptide Onc112 (residues 3-5, olive, PDB: 4ZER) (Seefeldt et al., 2015), and (D) the CMV-stalling peptidyl-tRNA (orange, PDB: 5A8L) (Matheisl et al., 2015). (E and F) Comparison of cryo-EM density (mesh) and model for Pro-Pro nascent chain (cyan ribbon) with (E) TnaC (yellow, PDB: 4UY8) (Bischoff et al., 2014), VemP (dark green, PDB: 5NWY) (Su et al., 2017) as well as (F) MifM (pink, PDB: 3J9W) (Sohmen et al., 2015) and SecM (tan, PDB: 3JBV) (Zhang et al., 2015). The relative position of nucleotide G2061 (grey) of the 23S rRNA is shown for reference.

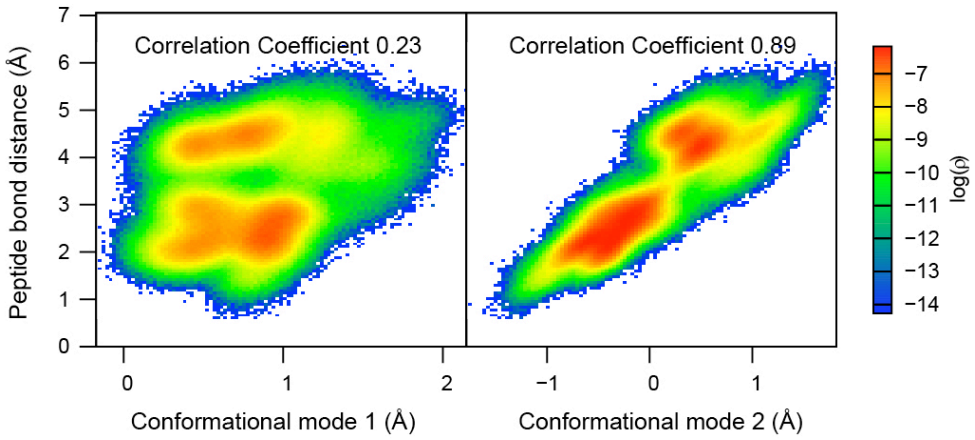

Figure S7 - Related to Figure 6. Conformation of polyproline nascent chain on the ribosome. Logarithm of the probability of finding a given peptide bond distance along the first (left panel) or the second (right) conformational mode of the CCA-end and the C-terminal proline backbone atoms obtained from all the simulations. Mode 2 highly correlates (cc=0.89) with the peptide bond distance, while mode 1 describes motions that are largely uncorrelated with the peptide bond distance (cc=0.23).